JMEPEG
https://doi.org/10.1007/s11665-024-09950-1

1059-9495/$19.00

ORIGINAL RESEARCH ARTICLE

Effect of Pre-Equal Channel Angular Pressing Homogenization on Microstructure and Mechanical Properties of As-Cast 7050 Al Alloy

Junjie Zhang, Tao He, Xiangyang Du, Yuanming Huo, Dongsheng Jia, and Xilin Chen

Submitted: 8 February 2024 / Revised: 5 June 2024 / Accepted: 11 June 2024

An effective homogenization scheme is crucial for successful room temperature equal channel angular pressing (RT-ECAP) deformation of the 7050 aluminum (Al) alloy. This study investigated the effects of different single-stage homogenization heat treatments (ST), double-stage homogenization heat treatments (DT) and subsequent RT-ECAP deformation on as-cast 7050 Al alloy. Multiscale observations of microstructure evolution were conducted using differential scanning calorimetry, optical microscopy, x-ray diffraction and scanning electron microscopy equipped with energy-dispersive spectroscopy. Mechanical properties and crack depth variations were analyzed using universal testing machine and depth testing platform. The results show that the microstructure of as-cast 7050 Al alloy exhibits severe dendritic segregation, with non-equilibrium phase areas fraction of approximately 4.1% and coarse grain boundaries around 5.14 µm. With increase in temperatures and times of ST, dendritic segregation gradually diminishes and the non-equilibrium second phase dissolves into the matrix. After DT of 7050 Al alloy at 465 °C-24 h+ 475 °C-4 h, only 0.7% of insoluble residual phases remained and the grain boundaries became fine with a width of 1.08 µm, representing reductions of approximately 82.9 and 79% compared to the as-cast, respectively. Additionally, owing to significant improvements in the microstructure, no cracks were observed in the subsequent RT-ECAP of 7050 Al alloy. The ultimate tensile strength (UTS) and yield strength (YS) of 7050 Al alloy decreased from (472±4) and (457±15) MPa in as-cast state to (450±17) and (335± 26) MPa after DT at 465 °C-24 h+475 °C-4 h. The fracture elongation of 7050 Al alloy was increased from (5.3±1.1) to (7.0±0.3)% in as-cast state. Subsequently RT-ECAP, the UTS and YS of 7050Al alloy were increased to (554±3) and (525±26) MPa, respectively, and the fracture elongation was reduced to (6.5± 0.3)%. After the DT of 465 °C-24 h+475 °C-4 h, significant improvements were achieved in the microstructure, simultaneously enhancing the plasticity and the RT-ECAP workability of 7050 Al alloy with limited strength reduction, indicating this scheme as the reasonable DT scheme.

Keywords as-cast 7050 Al alloy, ECAP, homogenization, mechanical properties, microstructure

1. Introduction

As a critical component widely employed in aerospace, new energy vehicles and other high-end equipment, the development of fasteners has emerged as a research focal point (Ref 1-3). Currently, fasteners are manufactured using titanium alloy and alloy steel as the primary raw materials (Ref 2, 4-6), making it difficult to simultaneously meet the increasingly pressing demand for both high-strength and lightweight characteristics simultaneously. Characterized by its low density and high specific strength, Al alloy has attracted increasing attention in the field of equipment manufacturing (Ref 7-10). The production and application of Al alloy fasteners have become a principal driving force for further advancements (Ref 11, 12). Nevertheless, Al alloy fasteners fail to meet the high-strength requirements such as aerospace and new energy vehicles, limiting its wide application. Therefore, there is significant importance in modifying the microstructure of Al alloys to achieve a substantial enhancement in the mechanical properties of their fasteners.

As a severe plastic deformation (SPD) technology, equal channel angular pressing (ECAP) has become a common method for the production of ultrafine-grained (UFG) and nanograin structured (NS) mechanical parts due to the cross section remains constant and repeatable (Ref 13-15). It has been shown that ECAP treatment of magnesium and alloys, copper, steel, Zn and titanium alloys can greatly increase their mechanical properties (Ref 16-19). Processing Al alloys through ECAP enables the manufacture of high-strength Al alloys (Ref 20-22). Heat-treatable 7050 Al alloy, due to the addition of a series of microalloying elements such as Cu, Mg, Zn and Si, increases certain mechanical properties and becomes a preferred material such as aircraft skins (Ref 23). However, during the cooling process of 7050 Al alloy casting, serious elemental segregation and the formation of a large number of

Junjie Zhang, Tao He, Xiangyang Du, Yuanming Huo, Dongsheng Jia, and **Xilin Chen**, School of Mechanical and Automotive Engineering, Shanghai University of Engineering Science, Shanghai, Songjiang 201620, China. Contact e-mail: hetao@sues.edu.cn.

Published online: 22 August 2024

non-equilibrium eutectic phases are produced due to the inhomogeneous distribution of the added alloying elements and insufficient solubility, which seriously affects the subsequent plastic deformation characteristics of the material and the mechanical properties of the processed products (Ref 24-27). It can be seen that before ECAP deformation, it is very necessary to carry out the corresponding treatment of as-cast 7050 Al alloy to eliminate or reduce the inhomogeneity in chemical composition and microstructure, thereby lowering the resistance to deformation and preparing the microstructure for deformation (Ref 28, 29).

Actually, homogenization treatment of alloys has become the most widely used process in order to improve RT workability. Wong et al. (Ref 30) studied cast AZ31B magnesium alloy and found that the homogenized treated alloy did not show surface cracking and exhibited improved machinability during subsequent plastic deformation. Yang et al. (Ref 31) and Deng et al. (Ref 32) found that homogenization improved its microstructure and facilitated subsequent rolling deformation on as-cast 7075 Al alloy and Al-Cu-Li-Zr alloy, respectively. Additionally, Liu et al. (Ref 33) conducted ST and DT on cast Mg-6Zn-3Sn alloys, demonstrating that DT could achieve better results. Gao et al. (Ref 34) pointed out that DT of Al-Cu could prevent overburning and subsequent high temperatures could further dissolve the residual eutectic phase. It can be observed that the DT effect is superior to ST, not only preventing the occurrence of overheating but also positively impacting the strength. However, the relationship between the effect of ST or DT on the microstructure of as-cast 7050 Al alloy and subsequent room temperature ECAP (RT-ECAP) plastic deformation has not been fully reported. It is essential to study the relationship between microstructure, mechanical properties and subsequent plastic deformation.

In this work, as-cast 7050 Al alloy was taken as the research object, the homogenization system of the alloy and the microstructure evolution during homogenization were investigated, the effects of different homogenization treatments on the RT-ECAP formability and mechanical properties of the alloy were explored, and the reasonable DT scheme was been established. The results of this research are expected to provide reliable theoretical guidance for establishing the homogenization regimen and enhancing the workability of RT-ECAP of as-cast 7050 aluminum alloy.

2. Material and Experimental Procedure

2.1 Material and Sample Preparation

In this paper, 7050 Al alloy ingot produced by Tong Xiang Metal Materials (Shanghai) Co., Ltd. was selected as the raw material with the chemical composition shown in Table 1. A number of 10-mm-diameter bars were cut from the original 7050 ingot Al alloy using an EDM wire cutter (DK 7735) as the initial as-cast samples.

Samples of as-cast 7050 Al alloy (approximately 10mg) were heated from 25 to 650 °C on a differential scanning calorimetry (DSC, STA 8000) at a constant heating rate of 10 °C/min to measure the phase transition temperature under nitrogen atmosphere. The result is shown in Fig. 1. The apparent heat endothermic peak of the curve at 495.5 °C is caused by the dissolution of the non-equilibrium eutectic phase within the as-cast 7050 Al alloy. Taking into account measurement errors, the overburning temperature for as-cast 7050 Al alloy can be set at 480 °C.

Then, the as-cast 7050 Al alloy was heat treated in a high-temperature furnace (SXL-1200D) at temperatures of 435, 465 and 480 °C with a heating rate of 10 °C/min, and holding times of 4, 8 and 10 h for a ST, respectively. On the basis of optimizing the ST regime, 7050 Al alloy was subjected to a second-stage homogenization with a heating temperature of 475 °C and holding times of 4, 8 and 10 h, respectively. The whole heat treatment was water quenching and the transfer time of the sample was within 3 s.

The cooled 7050 Al alloy was immediately put into an ECAP die with inner angle $\varphi=120°$ and outer angle $\psi=30°$. The ECAP forming of 7050 Al alloy was carried out at RT using a four-column hydraulic press (Y-160 T) with a descending speed of 3 mm/s. Meanwhile, MoS_2 was used as the lubricant for the ECAP experiments, in order to reduce the friction between 7050 Al alloy and the mold. The ECAP principle, equipment and the schematic diagram of the whole experimental route are presented in Fig. 2

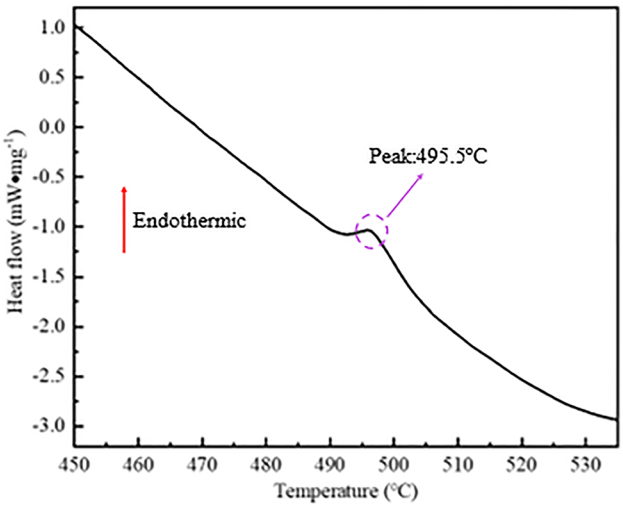

Fig. 1 DSC curve of as-cast 7050 Al alloy

Table 1 Chemical composition of 7050 Al alloy(wt.%)

Cu	Mg	Zn	Fe	Cr	Mn	Zr	Ti	Si	Al
2.0-2.6	1.9-2.6	5.7-6.7	≤ 0.15	≤ 0.04	≤ 0.10	0.08-0.15	≤ 0.06	≤ 0.12	Bal.

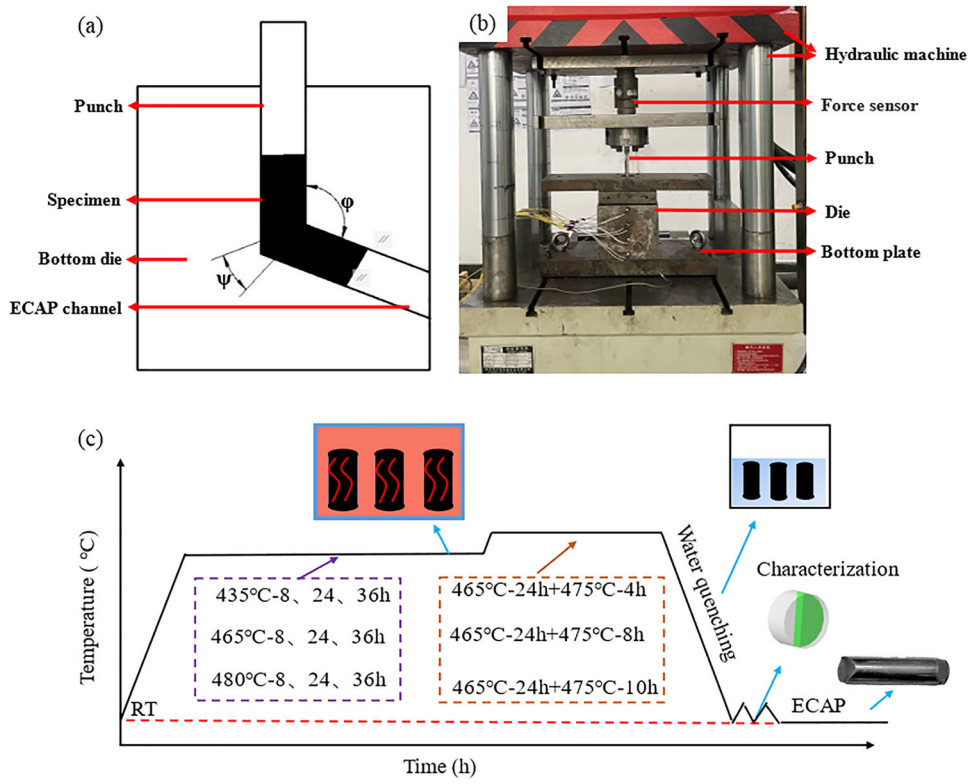

Fig. 2 (a) Principle diagram of ECAP; (b) forming equipment of ECAP; (c) Schematic diagram of the entire experimental route of 7050 Al alloy

2.2 Tensile Testing

Dog-bone shaped tensile test specimens of 30 mm × 6 mm × 1.2 mm (with a gauge length of 10 mm) were prepared using a wire EDM (DK7735). Sandpaper with polishing paste was used to grind and polish the tensile specimens, followed by cleaning and drying with an ultrasonic cleaner (G-040S). Tensile tests were performed on the specimens using a universal tensile testing machine (JVJ-50 s) with a tensile speed of 5 mm/min at RT. Three samples were tested for each condition to confirm reproducibility.

2.3 Microstructure Characterization

All of 7050 Al alloys after heat treatment were ground using 800, 1000, 1200, 1500 and 2000# sandpaper. Subsequently, mechanical polishing was performed on a polishing machine (MP-2B) using 2.0, 1.5 and 1.0 polishing pastes until a mirror finish was achieved. After polishing the specimens were chemically etched using Keller's reagent (1 mL HF+1.5 mL HCL+2.5 mL HNO_3+ 95 mL H_2O). Metallographic analysis of the corroded 7050 Al alloy was carried out using optical microscope (OM, 4X-CIS). The microstructure of the 7050 Al alloy was observed using a scanning electron microscope (SEM, QUANTA-250), and the microstructural composition was analyzed using attached energy-dispersive spectroscopy (EDS). X-ray diffraction (XRD) was used to analyze phases of the alloy samples, using Cu-Kα radiation, with a scanning speed of 8 min^{-1} and a scanning range of 10-90°. Field emission scanning electron microscopy (FE-SEM, QUANTA650) was used to observe the fracture morphology of 7050 Al alloy in different states. The grain morphology and dislocation density microstructure of 7050 Al alloy were observed by transmission electron microscopy (TEM, Talos F200X G2).

3. Results and Discussion

3.1 Microstructure of As-Cast 7050 Al Alloy

Figure 3 shows the microstructure morphology of as-cast 7050 Al alloy observed using SEM. It can be seen that coarse residual non-equilibrium phases are gathered at the grain boundaries in the as-cast microstructure. Quantitative measurements of the coarse grain boundaries, revealing an average width of approximately 5.14 μm.

Figure 4 shows the SEM images of the residual second phase morphology of the as-cast 7050 Al alloy and the corresponding EDS. The morphology of the residual second

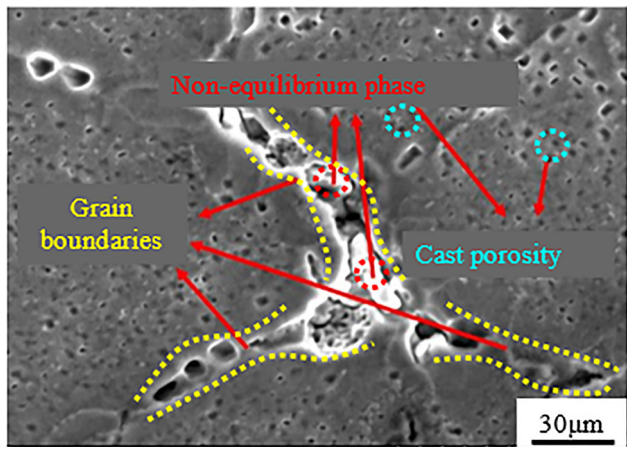

Fig. 3 Microstructure and morphology of as-cast 7050 Al alloy

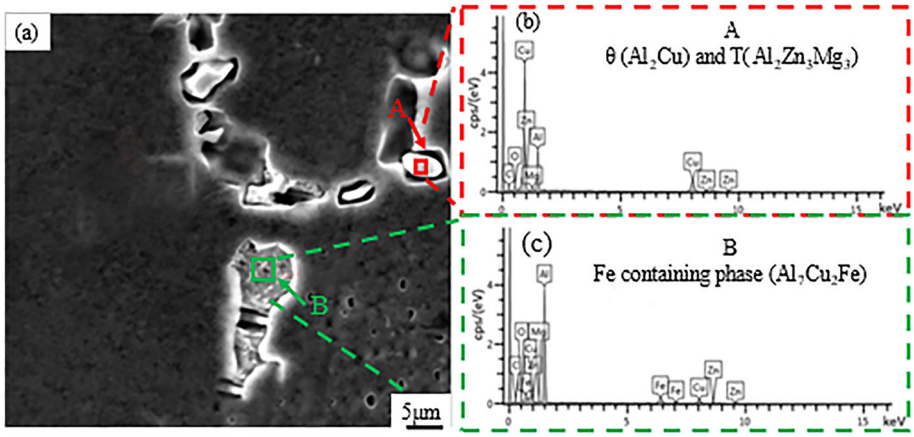

Fig. 4 Non-equilibrium phases of as-cast 7050 Al alloy: (a) SEM; (b–c) corresponding EDS

phase of the as-cast 7050 Al alloy, which is continuous or discrete in the microstructure and appears white and light white, as shown in Fig. 4(a). The quantitatively measured residual phase area fraction of the as-cast 7050 Al alloy is about 4.1%. In addition, the EDS results from point A show that the aggregated elements are mainly Al, Mg, Zn and Cu. Combining with the mass fractions of each element, it can be inferred to be composed of the θ (Al_2Cu) and T ($Al_2Zn_3Mg_3$) phases, as shown in Fig. 4(b). This is in agreement with the results of existing studies related to Al-Zn-Mg-Cu alloys (Ref 35, 36). From the EDS point scanning results at point B, it is seen that the aggregated elements have a certain content of Fe elements in addition to Cu, Mg, and Zn, which is deduced from the analysis to be mainly composed of the Fe-containing insoluble impurity phase (Al_7Cu_2Fe), as shown in Fig. 4(c). From the above analysis, it can be seen that it is necessary to eliminate the severe elemental segregation of as-cast 7050 Al alloy by homogenization.

3.2 Microstructures of 7050 Al Alloy After ST

Figure 5 shows the microstructure of as-cast 7050 Al alloy under different ST observed using optical microscopy (OM). From Fig. 5(a,b), the microstructure of as-cast 7050 Al alloy exhibits dendritic features, a radial distribution of grains, ambiguous grain morphology and grain boundary characteristics. Figure 5(c,d) shows the microstructure after 435 °C-10 h. The non-equilibrium residual phases begin to dissolve into the matrix and a small number of dendritic structural domains still exist. The heat enhances atomic activity in the 7050 Al alloy, facilitating the dissolution of residual phases at grain boundaries into the matrix. Figure 5(e,f) shows the microstructure after 465 °C-24 h, the dendritic structure is completely eliminated and the low melting point residual phase is basically dissolved. The microstructure of the alloy is smooth with continuous and distinct grain boundaries. However, there are still some high melting point residual phases that have not been dissolved. When the holding time was extended to 36 h, the microstructure did not show significant differences compared to that at 24 h, as shown in Fig. 5(g,h). From the above analysis, it can be deduced that 465 °C-24 h can be used as a reasonable first-stage homogenization regime.

3.3 Microstructures of 7050 Al Alloy after DT

As shown in the above results, the low melting point eutectic phases present in 7050 Al alloy have dissolved into the matrix at 465 °C-24 h regime. In order to dissolve the high melting point non-equilibrium such as S(Al_2CuMg) phase, a second-stage homogenization of the Al alloy is required. The microstructures of 7050 Al alloy treated by DT with different holding times at the second-stage temperature of 475 °C are shown in Fig. 6. After 465 °C-24 h+475 °C-1 h homogenization, the high melting point non-equilibrium at the grain boundary starts to dissolve into the matrix gradually and the grain boundary becomes obviously continuous and clear, as shown in Fig. 6(a,b). With the holding time extended to 4 h, more high melting point non-equilibrium phases dissolve, the grains tend to be equiaxed crystals, as shown in Fig. 6(c). Extending the holding time to 8 h does not result in a significantly different improvement in microstructure morphology compared to that observed at 4 h, as shown in Fig. 6(d). Meanwhile, the microstructure of 7050 Al alloy under the 8 h shows the appearance of grain boundary triangular re-melting zone (region A) and re-melting sphere (region B), as shown in Fig. 6(d). The appearance of region A and B indicates that the overburning behavior of as-cast 7050 Al alloy has been occurred at 465 °C-24 h+475 °C-8 h.

Figure 7 shows the SEM images of as-cast 7050 Al alloy after DT at 465 °C-24 h+475 °C-4 h with the corresponding EDS mapping distribution of elements. SEM images show that the microstructure of the 7050 Al alloy appears smooth. The grain boundaries changes from coarse to fine with a width of 1.08 μm. The EDS shows that the aggregation of Mg, Zn and Cu elements in the as-cast 7050 Al alloy becomes homogeneously distributed after 465 °C-24 h+475 °C-4 h. Besides, a small amount of Fe, Cu and Si elements are still observed to be aggregated from the EDS scanning. The residual elements consist of insoluble impurity phases of Al_7Cu_2Fe and Mg_2Si, scattered sporadically in the microstructure of 7050 Al alloy, in agreement with previous research results (Ref 35, 37, 38). Additionally, quantitative analysis of the 7050 Al alloy treated with DT at 465 °C-24 h+475 °C-4 h revealed that the area fraction of the residual phases is approximately 0.7%. Apart from a few refractory impurity phases remaining undissolved, most of the eutectic phases have fully dissolved into the matrix.

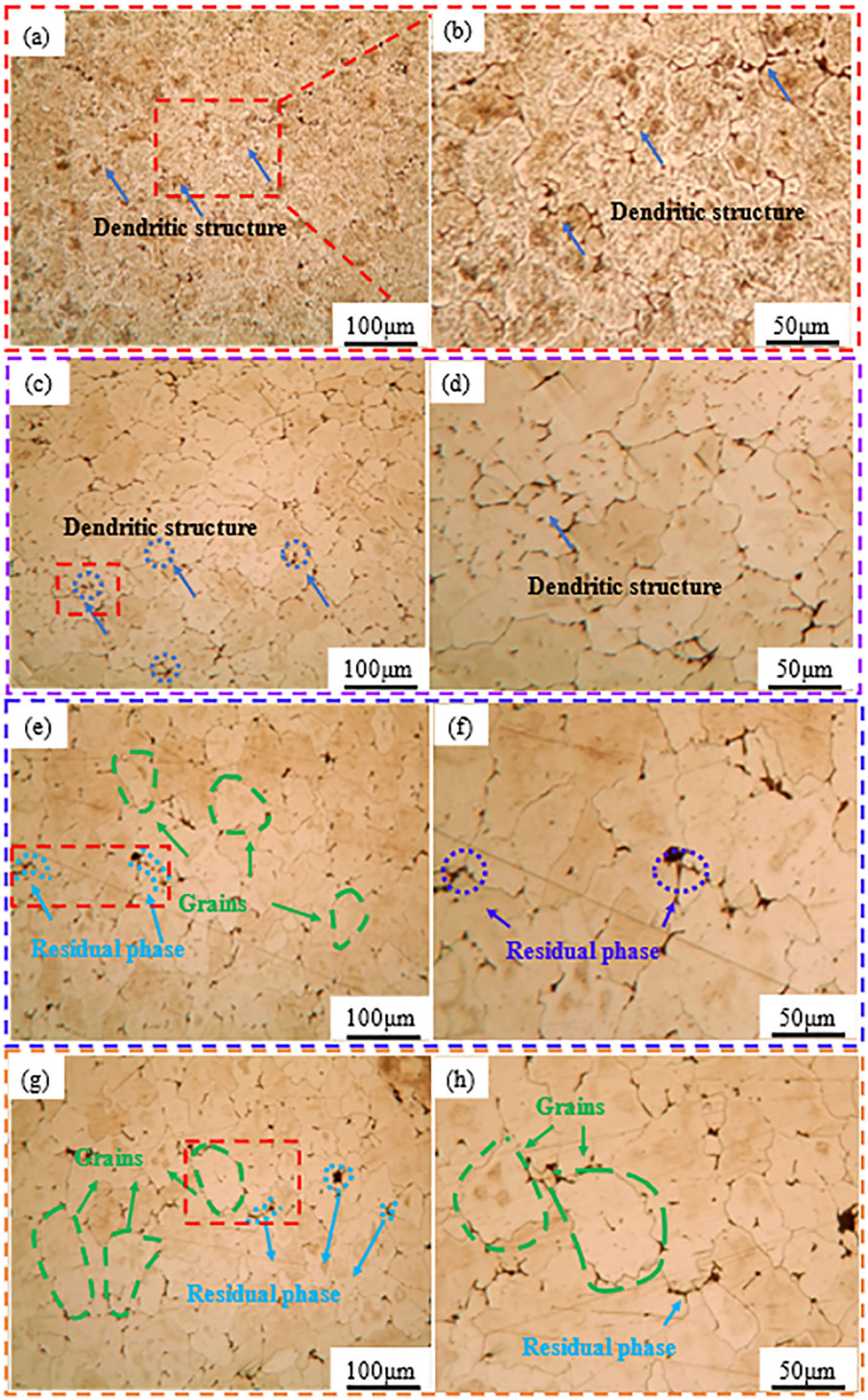

Fig. 5 OM images of ST of 7050 Al alloy and enlarged images of the area in marked by the red frame: (a-b) as-cast; (c-b) 435 °C-10 h; (e-f) 465 °C-24 h; (g-h) 465 °C-36 h (Color figure online)

Moreover, the overburning behavior caused by longer holding time is avoided. Then, the optimal DT scheme for the as-cast 7050 Al alloy is 465 °C-24 h+475 °C-4 h.

3.4 X-Ray Diffraction Analysis

XRD patterns of as-cast 7050 Al alloy after different ST are shown in Fig. 8. A large amount of η ($MgZn_2$) phase exists in the as-cast 7050 Al alloy. With the increase in temperature with holding times, the η phase gradually dissolves into the matrix and forms the S phase, as shown in Fig. 8(a,b). From Fig. 8(c), it can be seen that only the α(Al) peak is observed in the as-cast 7050 Al alloy at 480 °C for different holding times and no other distinct characteristic peaks are seen, indicating the disappearance of other soluble intermetallic compounds. Combining the analysis of OM and XRD plots, the scheme of 465 °C-24 h as the first-stage of homogenization is reasonable.

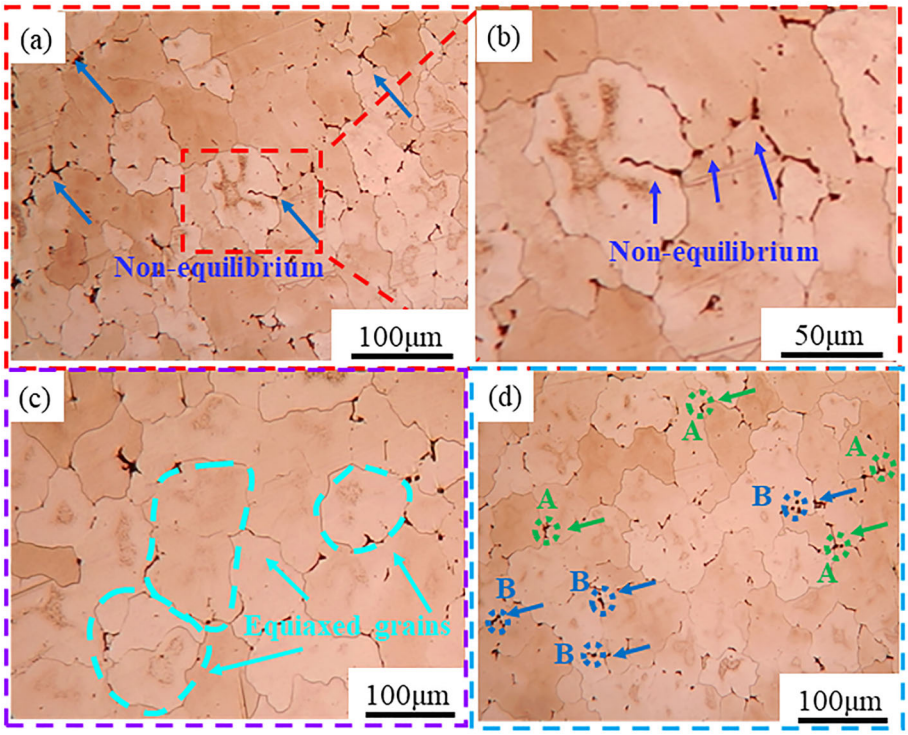

Fig. 6 OM images of 7050 Al alloy after different DT: (a) 465 °C-24 h+475 °C-1 h; (b) enlarged image of the area in (a) marked by the red frame; (c) 465 °C-24 h+475 °C-4 h; (d) 465 °C-24 h+475 °C-8 h (Color figure online)

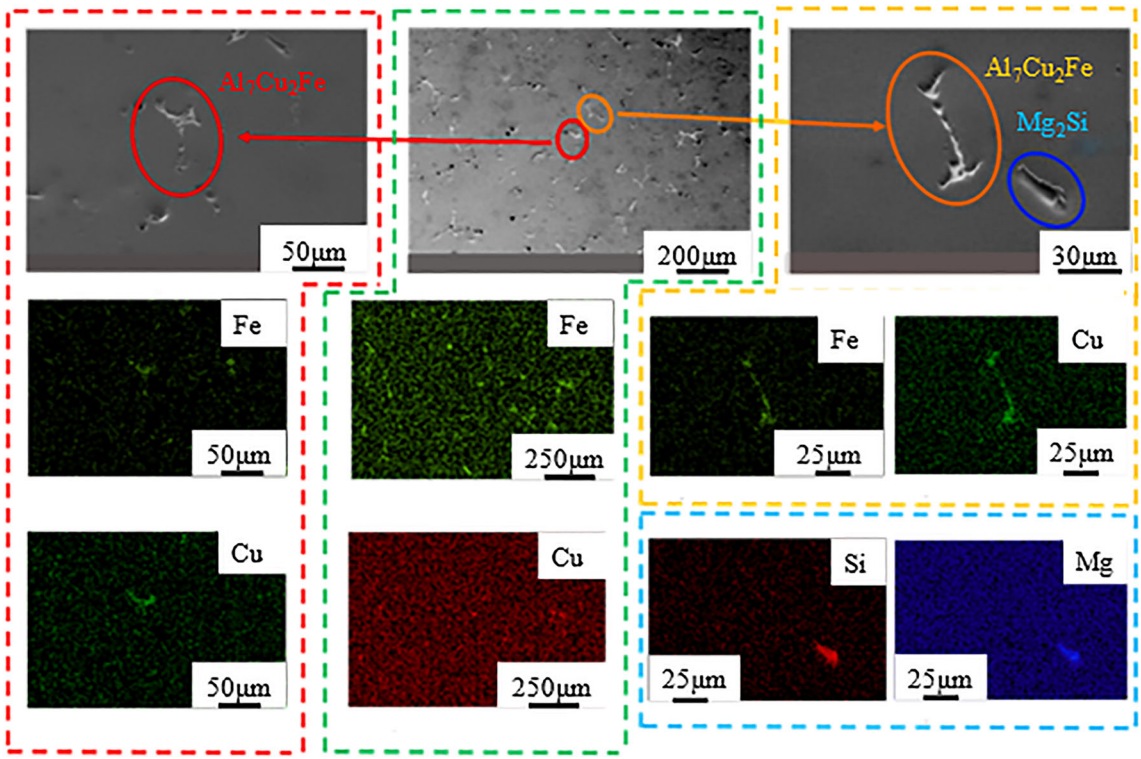

Fig. 7 SEM and EDS images of 7050 Al alloy after homogenization of 465 °C-24 h+475 °C-4 h

Figure 9 shows the XRD pattern of 7050 Al alloy after DT at 465°C-24 h+475°C-4 h. It can be found that both the low melting point η phase and the high melting point phase are fully dissolved into the matrix, leaving the Mg_2Si insoluble phase. Meanwhile, the indissolvable phase Al_7Cu_2Fe in alloy 7050 could not be detected by XRD due to its low content, which is consistent with the results of the related study (Ref 39, 40). On

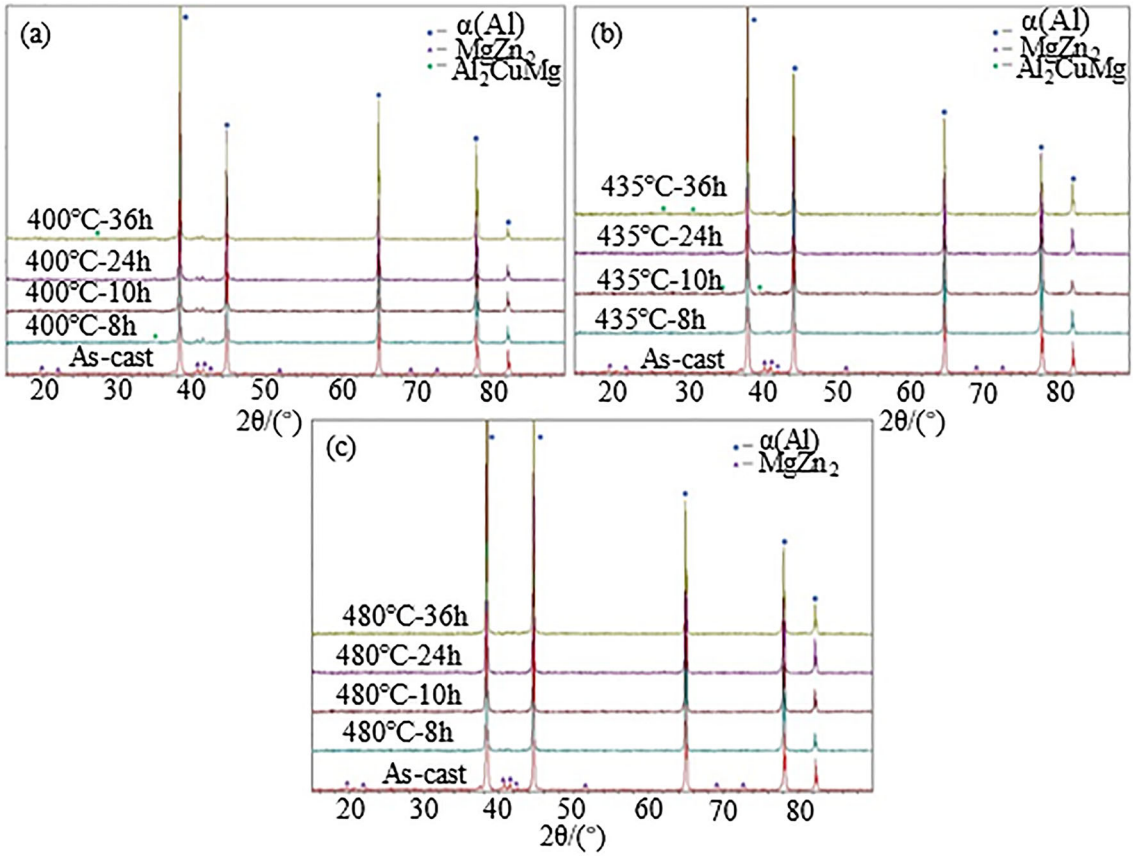

Fig. 8 XRD patterns of 7050 Al alloy after different ST temperatures and times: (a) 400 °C; (b) 435 °C; (c) 480 °C

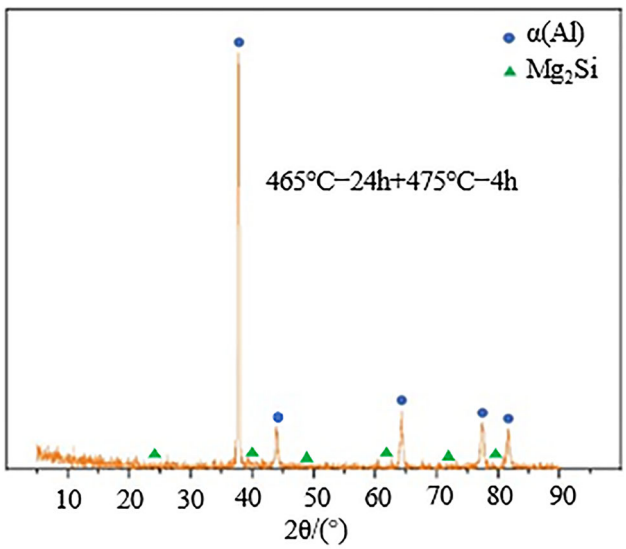

Fig. 9 XRD pattern of 7050 Al alloy after 465 °C-24 h+475 °C-4 h

the whole, the suitable DT scheme for the 7050 Al alloy is suggested to be 465 °C-24 h+475 °C-4 h.

3.5 Morphology and Crack Depth of RT-ECAP 7050 Al Alloy

Figure 10(a) and (b) shows the surface morphology and fracture depth of as-cast 7050 Al alloy during RT-ECAP deformation after different homogenization. After 435 °C-8 h, 7050 Al alloy undergoes complete shear fracture in the subsequent ECAP deformation and the crack depth is equal to the size of the initial diameter, which is about 10 mm. When the temperature is increased to 465 °C, the 7050 Al alloy does not undergo complete fracture, but the crack is also deep, which is 8.31mm. Further extending the holding time to 24 h, the 7050 Al alloy shows a reduction in crack depth and number in the ECAP, which was 3.95 mm, a reduction of approximately 60.5%. After DT of 465 °C-24 h+475 °C-1 h, the subsequent ECAP deformation of the 7050 Al alloy showed only one crack with a depth of 2.68mm, a reduction of 73.2%. During the ECAP deformation after DT at 465 °C-24 h+475 °C-4 h, 7050 Al alloy does not show obvious defects such as cracks, enhancing the RT-ECAP workability.

In order to further understand the relationship between the subsequent ECAP deformation and the microstructure of the 7050 Al alloy after different homogenization, the fracture modes of different states of the 7050 Al alloy during ECAP were investigated by FE-SEM. Figure 11 shows the FE-SEM images of the fracture shapes of different states of 7050 Al alloy in subsequent ECAP deformation. After ST at 435 °C-8 h, the presence of a large number of dendritic structures and non-equilibrium eutectic phases in the 7050 Al alloy resulted in poor ductility, which led to the appearance of flat facets and fracture cracks in the subsequent ECAP fracture morphology, which showed brittle fracture dominant fracture mode, as shown in Fig. 11(a). When the ST temperature was increased to 465 °C, the microstructure was effectively improved with the appearance of unevenly distributed dimples, showing a mixed

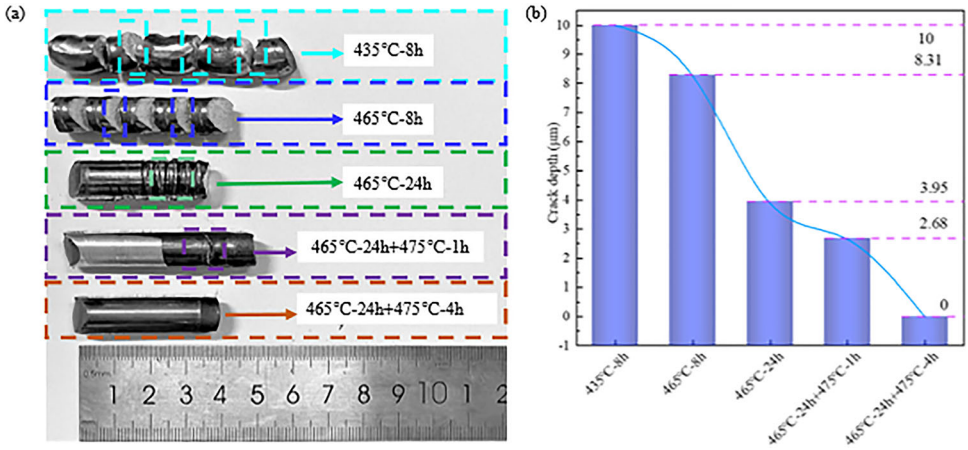

Fig. 10 ECAP deformation of 7050 Al alloy after different homogenization schemes: (a) deformation morphology; (b) crack depth changes

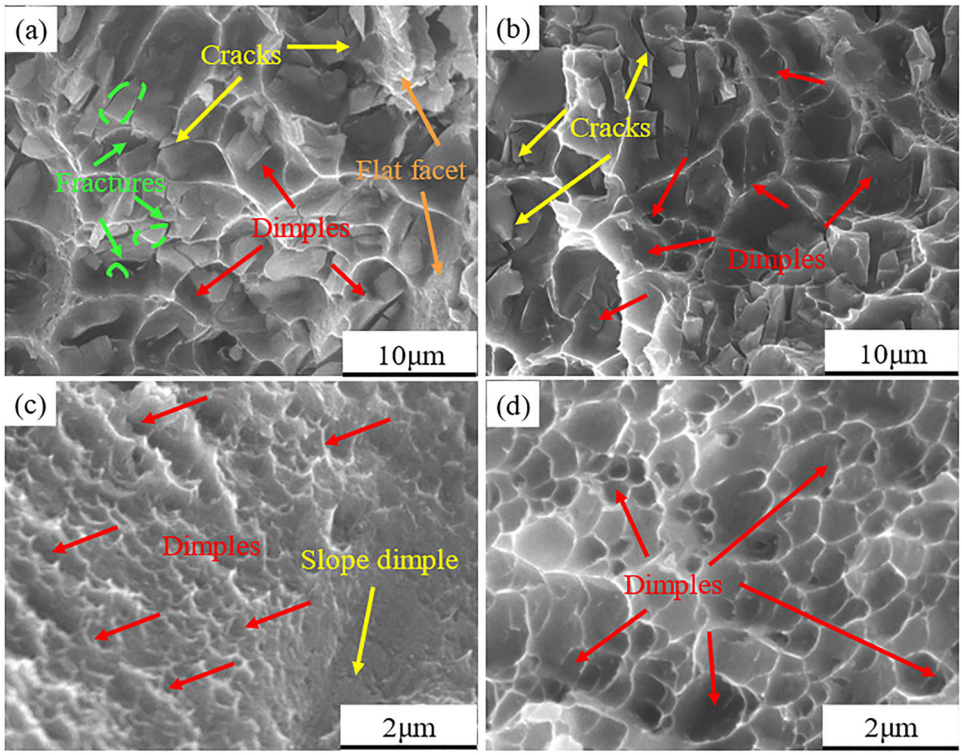

Fig. 11 FE-SEM images of fracture morphologies of different 7050 Al alloy states: (a) 435 °C-8 h; (b) 465 °C-8 h; (c) 465 °C -24 h; (d) 465 °C-24 h+475 °C-1 h

fracture of ductile and brittle fracture, as shown in Fig. 11(b). After 465 °C-24 h, with the disappearance of dendritic structures and the dissolution of low melting point non-equilibrium phases into the matrix, a large number of dimples and a ridge shape appear in the subsequent ECAP fracture morphology, representing ductile fracture, as shown in Fig. 11 (c). Figure 11(d) shows the ECAP fracture morphology of 7050 after DT at 465 °C-24 h+475 °C-1 h. It can be seen that due to the dissolution of some of the high melting non-equilibrium phase, a large number of dimples and ridges appear and are more homogeneously distributed. The more homogeneously distributed dimples indicate that the plasticity of the alloy is greatly improved. It can be further speculated that the ductility of 7050 Al alloy will be further improved after the DT at 465 °C-24 h+475 °C-4 h, when the remaining high melting point non-equilibrium is resolved and the microstructure reaches the ideal state, which is in agreement with the results of microstructure evolution. Therefore, 465 °C-24+475 °C-4 h can be considered a reasonable DT scheme for as-cast 7050 aluminum alloy.

3.6 Mechanical Properties of 7050 Al Alloy in Different States

To investigate the influence of homogenization and ECAP on the mechanical properties of 7050 Al alloy, RT tensile tests were conducted and the results are shown in Fig. 12(a) and (b). The ultimate tensile strength (UTS) and yield strength (YS) of

7050 Al alloy decreased from (472±4) and (457±15) MPa in as-cast state to (450±17) and (335±26) MPa after DT at 465 °C-24 h+475 °C-4 h. At the same time, the fracture elongation of 7050 Al alloy was increased from (5.3±1.1) to (7.0±0.3)% in as-cast state. Besides, after ECAP, the UTS and YS of 7050 Al alloy were increased to (554±3) and (525±26) MPa, respectively, and the fracture elongation was reduced to (6.5±0.3)%, as shown in Fig. 12(b).

The grain size distribution of 7050 Al alloy in different states is shown in Fig. 13(a). Under the thermal driving force provided by the DT at 465 °C-24 h+475 °C-4 h, the diffusion of solute atoms of 7050 Al alloy is accelerated and complete recrystallization occurs. Additionally, the dissolution of the non-equilibrium second phase aggregated at the grain boundaries into the matrix induces an increase in grain size from (27.6±2.4) to (107.7±9.6) μm in the as-cast state, which is consistent with the microstructure evolution results. Figure 13(b) shows the BF-TEM image of 7050 Al alloy after DT at 465 °C-24 h+475 °C-4 h. Due to the high temperature, dislocations undergo annihilation behavior and coarse grains are observed, but dislocations are difficult to observe, which is consistent with existing studies. The dislocation density of metal alloys is closely related to grain size and mechanical properties. Therefore, the decrease in dislocation density with increase in grain size reduces the obstacle of dislocation movement and the deformation resistance, which causes a decrease in UTS and YS and an increase in fracture elongation of 7050 Al alloy, which is in accordance with the Hall–Petch relationship and the Bailey–Hirsch dislocation relationship (Ref 14, 15, 41). Furthermore, during the subsequent ECAP process, due to the shear force induced continuous dynamic recrystallization (CDRX) of 7050 Al alloy, the grain refinement shows a lath-like shape with a size of (24.7±1.1) μm. At the same time, a large amount of dislocation density reappears as shown in Fig. 13(c). The decrease in grain size and the increase in dislocation density increase the barrier to dislocation movement and the resistance to tensile deformation, resulting in an increase in strength and a decrease in fracture elongation of the 7050 Al alloy.

In summary, the DT at 465 °C-24 h+475 °C-4 h improve the microstructure characteristics of as-cast 7050 Al alloy, significantly enhancing RT-ECAP deformability with minimal reduction in tensile strength. Besides, subsequent ECAP deformation further increased the strength (including UTS and YS), expanding its application prospects. Consequently, by evaluating the microstructure characteristics, mechanical properties and RT-ECAP deformation behavior of the 7050 Al alloy comprehensively, it is reasonable to conclude that the DT of 465 °C-24 h+475 °C-4 h represents the most effective homogenization scheme.

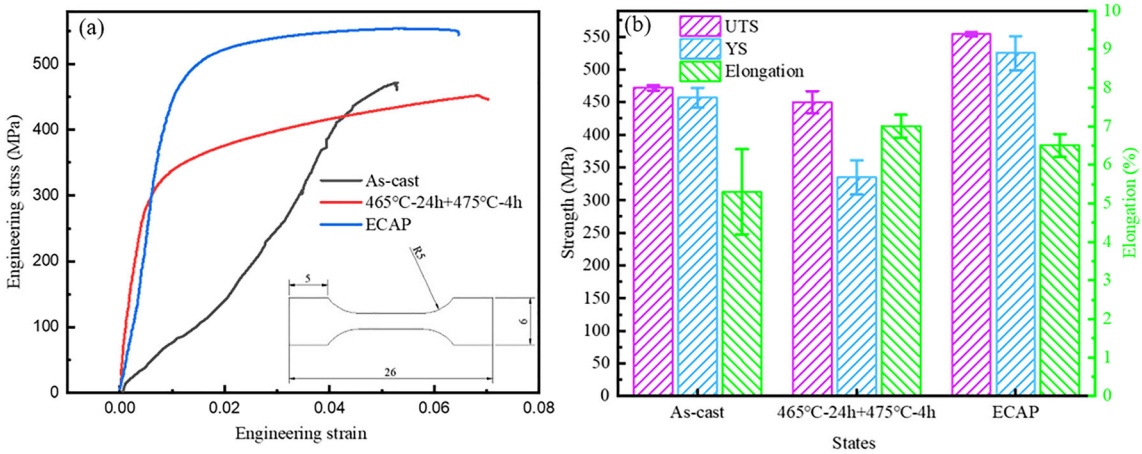

Fig. 12 Mechanical properties of 7050 Al alloy in different states: (a) engineering stress–strain curves; (b) tensile properties

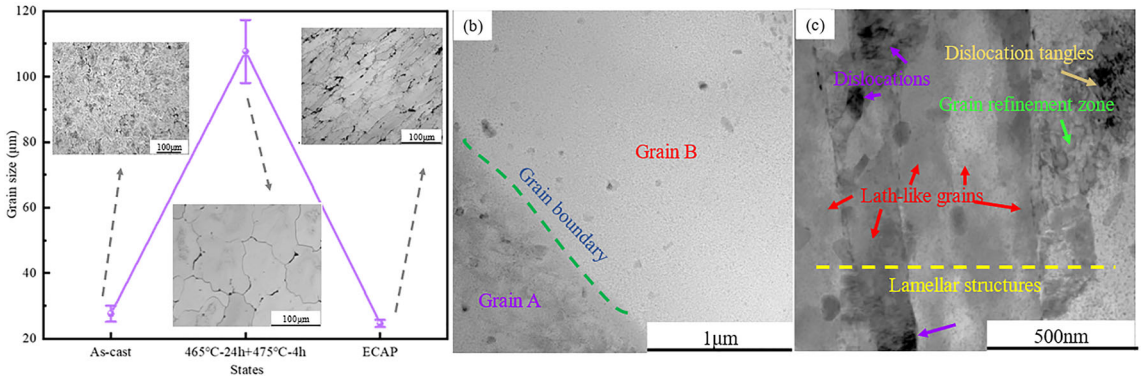

Fig. 13 Grain size distribution of 7050Al alloy in different states (a); BF-TEM images of 7050 Al alloy in 465 °C-24 h+475 °C-4 h state (b) and ECAP state (c)

4. Conclusions

In this study, as-cast 7050 Al alloy was subjected to different regimes of ST, DT and subsequent RT-ECAP deformation, observing microstructure evolution, damage crack depth and tensile strength, revealing the relationship between microstructure and ECAP deformation behavior. The following main conclusions can be drawn:

1. The element distribution in the as-cast 7050 Al alloy is inhomogeneous, with severe dendritic segregation. The area of non-equilibrium residual phases in the as-cast alloy is approximately 4.1%, with a grain boundary width of 5.14μm.
2. During the homogenization of the as-cast 7050 Al alloy, low melting non-equilibrium phases continuously dissolve into the matrix. After the 465 °C-24 h+475 °C-4 h treatment, dendritic segregation in the as-cast 7050 Al alloy is eliminated and the distribution of elements from the grain boundaries to inside becomes homogeneous. The alloy contains approximately 0.7% insoluble impurity phases and the grain boundary width narrows to about 1.08μm, representing reductions of 82.9% and 79% compared to the as-cast state, respectively.
3. After ST at 465 °C-8 and 24 h, the ECAP crack depth of 7050 decreased from 10 to 8.31 and 3.95 mm, reducing by about 16.9% and 60.5%, respectively. In the DT at 465 °C-24 h+475 °C-4 h, cracks in 7050 Al alloy disappear, resulting in optimal ECAP formability.
4. The UTS and YS of the 7050 Al alloy decrease from (472±4) and (457±15) MPa in the as-cast state to (450 ±17) and (335±26) after DT at 465 °C-24 h+475 °C-4 h, respectively. The fracture elongation of 7050 Al alloy increases from (5.3±1.1) to (7.0±0.3)% in as-cast state. Subsequent ECAP deformation results in an increased UTS and YS of (554±3) and (525±26) MPa, respectively. The 465 °C-24 h+475 °C-4 h scheme can be determined as the optimal DT for the as-cast 7050 Al alloy.

Acknowledgments

This study is supported by the National Science Foundation of China (Grant No.52275350) and Natural Science Foundation Project of Shanghai (Grant No.20ZR1422100)

References

1. W.H. Li, S.J. Guo, Y.D. Liu, Z.Q. Shen, Y. Xiong, F. Gao, D.J. Hughes, and J. Lin, Structure Health Monitoring of Composites Joint Reinforced by Acoustic Emission based Smart Composite Fasteners, *Compos. Commun.*, 2022, **33**, p 101213. (**in English**)
2. Y. Qi, X.B. Zhang, L.L. Shan, G.M. Jiao, Q.W. Gao, Z.L. Lin, W.B. Zheng, and S. Zhao, Design and Fabrication of Isotropic High-Strength Ti-6Al-4V Fastener, *Mater. Lett.*, 2022, **323**, p 132554. (**in English**)
3. C.X. Yao, Z.C. Qi, and W.L. Chen, Lightweight and High-Strength Interference-Fit Composite Joint Reinforced by Thermoplastic Composite Fastener, *Thin Wall. Struct.*, 2022, **179**, p 109471. (**in English**)
4. W.B. Yang, H.Y. Ming, T. He, Y. Xue, Y.J. Hu, and M.L. Sheng, Microstructure Evolution of TC16 Titanium Alloy for Producing Aerospace Fasteners during Cold Compression, *Rare Met. Mater. Eng.*, 2022, **51**(2), p 386–391. (**in English**)
5. H.C. Lee, Y.G. Jin, Y.H. Lee, I.H. Son, D.L. Lee, and Y.T. Im, Process Design of High-Strength Bolt of Fully Pearlitic High-Carbon Steel, *J. Mater. Process. Technol.*, 2010, **210**(14), p 1870–1875. (**in English**)
6. J.S. Kim, Y.H. Lee, D.L. Lee, K.T. Park, and C.S. Lee, Microstructural Influences on Hydrogen Delayed Fracture of High Strength Steels, *Mater. Sci. Eng. A*, 2009, **505**(1–2), p 105–110. (**in English**)
7. J.J. Zhang, T. He, Y.M. Huo, X.Y. Du, and X.L. Chen, Study on Grain Growth Kinetics during Homogenization Process of As-Cast 7075 Aluminum Alloy, *J. Plast. Eng.*, 2023, **30**(12), p 184–191. (**in Chinese**)
8. J.Y. Gao, T. He, Y.M. Huo, M. Song, T. Yao, and W. Yang, Comparison of Modified Mohr-Coulomb Model and Bai-Wierzbicki Model for Constructing 3D Ductile Fracture Envelope of AA6063, *Chin. J. Mech. Eng.*, 2021, **34**(2), p 35. (**in English**)
9. B.S. Gong, Z.J. Zhang, J.P. Hou, Q.Q. Duan, X.G. Wang, and Z.F. Zhang, Effect of Aging State on Corrosion Fatigue Properties of 7075 Aluminum Alloy, *Int. J. Fatigue*, 2022, **161**, p 106916. (**in English**)
10. S.H. Kayani, J.G. Jung, M.S. Kim, and K.J. Euh, Effect of Cooling Rate on Precipitation Behavior of Al–7.65Zn–2.59Mg–1.95Cu Alloy with Minor Elements of Zr and Ti, *Met. Mater. Int.*, 2020, **26**(7), p 1–8. (**in English**)
11. J.J. Pang, F.C. Liu, J. Liu, M.J. Tan, and D.J. Blackwood, Friction Stir Processing of Aluminium Alloy AA7075: Microstructure, Surface Chemistry and Corrosion Resistance, *Corros. Sci.*, 2016, **106**(5), p 217–228. (**in English**)
12. P.A. Rometsch, Y. Zhang, and S. Knight, Heat Treatment of 7xxx Series Aluminium Alloys—Some Recent Developments, *Trans. Nonferrous Met. Soc. China*, 2014, **24**, p 2003–2017. (**in English**)
13. D.S. Jia, T. He, M. Song, Y.M. Huo, and H.Y. Hu, Effects of Equal Channel Angular Pressing and Further Cold Upsetting Process to the Kinetics of Precipitation during Aging of 7050 Aluminum Alloy, *J. Mater. Res. Technol.*, 2023, **26**, p 5126–5140. (**in English**)
14. G.S. Li, X.Y. Pan, J. Jiang, J.H. Li, L.L. Xie, H.T. Liu, and M.Y. Zhang, Achieving Ultra-Fine Grains and High Corrosion Resistance of Al–Zn–Mg–Cu Alloy by ECAP and Post Cold Rolling, *J. Mater. Res. Technol.*, 2023, **26**, p 7354–7368. (**in English**)
15. G.S. Li, S. Xu, T. Wan, H. Liu, L. Xie, M. Zhang, and J. Li, Effect of Intermediate-Temperature Severe Plastic Deformation on Microstructure Evolution, Mechanical Properties and Corrosion Behavior of an Al-Zn-Mg-Cu Alloy, *Mater. Charact.*, 2023, **205**, p 113248.
16. G.M. Claudia, G. Ivan, O.M. Laia, J.P. Emilio, G. Maria-Pau, V. Maurizio, C.J. Luís, and P. Marta, Influence of ECAP Process on Mechanical, Corrosion and Bacterial Properties of Zn-2Ag Alloy for Wound Closure Devices, *Mater. Des.*, 2023, **228**, p 111817. (**in English**)
17. Y. Gu, A. Ma, J. Jiang, H. Li, D. Song, H. Wu, and Y. Yuan, Simultaneously Improving Mechanical Properties and Corrosion Resistance of Pure Ti by Continuous ECAP Plus Short-Duration Annealing, *Mater. Charact.*, 2018, **138**, p 38–47. (**in English**)
18. C. Sun, H. Liu, C. Wang, J. Ju, G. Wang, J. Jiang, A. Ma, J. Bai, F. Xue, and Y.C. Xin, Anisotropy Investigation of an ECAP-Processed Mg-Al-Ca-Mn Alloy with Synergistically Enhanced Mechanical Properties and Corrosion Resistance, *J. Alloys Compd.*, 2022, **911**, p 165046. (**in English**)
19. Y. Zhang, W. Rong, Y.J. Wu, and L.P. Peng, Achieving Ultra-High Strength in Mg–Gd–Ag–Zr Wrought Alloy via Bimodal-Grained Structure and Enhanced Precipitation, *J. Mater. Sci. Technol.*, 2020, **54**, p 160–170. (**in English**)
20. Y.G. Jin, H.M. Baek, S.K. Hwang, Y. Im, and B.C. Jeon, Continuous High Strength Aluminum Bolt Manufacturing by the Spring-Loaded ECAP System, *J. Mater. Process. Technol.*, 2012, **212**(4), p 848–855. (**in English**)
21. J.H. Kim, S.K. Hwang, Y. Im, I. Son, and C.M. Bae, High-Strength Bolt-Forming of Fine-Grained Aluminum Alloy 6061 with a Continuous Hybrid Process, *Mater. Sci. Eng. A*, 2012, **552**, p 316–322. (**in English**)
22. D.S. Jia, T. He, M. Song, Y.M. Huo, X.Y. Du, V. Aleksey, J. Li, and H. Y. Hu, Microstructure Evolution of 7050 Al Alloy Fasteners during Cold Upsetting after Equal Channel Angular Pressing, *J. Cent. South Univ.*, 2023, **30**(11), p 3682–3695. (**in English**)
23. W.J. Zhang, R.M. Su, G.L. Li, and Y.D. Qu, Effect of Pre-aging Process on Microstructure and Properties of 7075–T8 Aluminium Alloy, *J. Alloys Compd.*, 2023, **960**, p 170953. (**in English**)

24. J.W. Cha, S.C. Jin, J.G. Jung, and S.H. Park, Effects of Homogenization Temperature on Microstructure and Mechanical Properties of High-Speed-Extruded Mg–5Bi–3Al Alloy, *J. Magnes. Alloys*, 2022, **10** (10), p 2833–2846. (**in English**)
25. J.B. Liu, K. Zhang, J.T. Han, X.G. Li, Y.J. Li, M.L. Ma, J.W. Yuan, and M. Li, Homogenization Heat Treatment of Mg–7.0 wt.%Y–1.0 wt.% Nd–0.5 wt.%Zr alloy, *Rare Met.*, 2015, **39**(10), p 1196–1201. (**in English**)
26. T. Nakata, C. Xu, Y. Ito, and S. Kamado, Role of Homogenization on Tensile Properties and Microstructures in a Dilute Mg–Zn–Ca–Mn Alloy Sheet, *Mater. Sci. Eng. A*, 2022, **833**, p 142541. (**in English**)
27. L. Hua, X. Hu, and X. Han, Microstructure Evolution of Annealed 7075 Aluminum Alloy and Its Influence on Room-Temperature Plasticity, *Mater. Des.*, 2020, **196**, p 109192. (**in English**)
28. Y. Totik, R. Sadeler, I. Kaymaz, and M. Gavgali, The Effect of Homogenisation Treatment on Cold Deformations of AA 2014 and AA 6063 Alloys, *J. Mater. Process. Technol.*, 2004, **147**, p 60–64. (**in English**)
29. X. Fan, D. Jiang, and Q. Meng, The Microstructural Evolution of an Al-Zn-Mg-Cu Alloy during Homogenization, *Mater. Lett.*, 2006, **60** (12), p 1475–1479. (**in English**)
30. T.W. Wong, A. Hadadzadeh, M.J. Benoit, and M.A. Wells, Impact of Homogenization Heat Treatment on the High Temperature Deformation Behavior of Cast AZ31B Magnesium Alloy, *J. Mater. Process. Technol.*, 2018, **254**, p 238–247. (**in English**)
31. H.F. Yang, R.S. Huang, Y.L. Zhang, M.N. Li, S. Koppala, P. Kemacheevakul, and J. Sannapaneni, Effect of Rolling Deformation and Passes on Microstructure and Mechanical Properties of 7075 Aluminum Alloy, *Ceram. Int.*, 2023, **49**(1), p 1165–1177. (**in English**)
32. Y.L. Deng, J.J. Xu, J.Q. Chen, and X.B. Guo, Effect of Double-Step Homogenization Treatments on the Microstructure and Mechanical Properties of Al–Cu–Li–Zr Alloy, *Mater. Sci. Eng. A*, 2020, **795**, p 1–21. (**in English**)
33. Y.H. Liu, X.G. Li, Y.J. Li, G.L. Shi, J.W. Yuan, and K. Zhang, Homogenization Treatment of Mg-6Zn-3Sn (wt.%) Alloy and Its Effects on Microstructure and Mechanical Properties, *Trans. Nonferrous Metal. Soc. China*, 2023, **33**(1), p 67–78. (**in English**)
34. Y.H. Gao, J. Kuang, G. Liu, and J. Sun, Effect of Minor Sc and Fe Co-Addition on the Microstructure and Mechanical Properties of Al-Cu Alloys during Homogenization Treatment, *Mater. Sci. Eng. A*, 2019, **746**(11), p 11–26. (**in English**)
35. R.S. Huang, H.F. Yang, S.J. Zheng, M.N. Li, H. Wang, Y.H. Duan, C.F. Yue, and C. Yang, The Evolution Mechanism of the Second Phase during Homogenization of Al-Zn-Mg-Cu Aluminum Alloy, *Mater. Des.*, 2023, **235**, p 1–11. (**in English**)
36. V.V. Bryukhovetsky, D.E. Myla, V.P. Poyda, and A.V. Poyda, Effect of Homogenization on the Superplasticity and Microsuperplasticity of the Al-Zn-Mg-Cu Aluminum Alloy, *J. Nano Electron. Phys.*, 2020, **12**(6), p 1–8. (**in English**)
37. H.Q. Teng, B.Q. Xiong, Y.A. Zhang, H.W. Liu, and X. He, Zn □□ Al-Zn-Mg-Cu 系铝合金的凝固态显微组织(Solidification Microstructure of High Zinc-Containing Al-Zn-Mg-Cu Alloys), *Trans. Nonferrous Met. Soc. China*, 2015, **25**(04), p 852–865. (**in Chinese**)
38. X.X. Yuan, D.F. Yin, X.X. Yu, K.G. Pan, T. Hu, Z.F. Lv, and Z.F. Zhu, Al-Zn-Mg-Cu-Zr-01.2Ce合金铸锭的均匀化退火及组织演变 (Homogenization Treatment of As-Cast Al-Zn-Mg-Cu-Zr-01.2Ce Aluminum Alloy and Microstructure Evolution during Homogenization), *Trans. Nonferrous Met. Soc. China*, 2017, **27**(03), p 459–467. (**in Chinese**)
39. Y.J. Guo, J.F. Li, D.-D. Lu, S.X. Deng, G.J. Zeng, Y.L. Ma, W. You, Y. L. Chen, X.H. Zhang, and R.F. Zhang, Characterization of Al_3Zr Precipitation Via Double-Step Homogenization and Recrystallization Behavior after Subsequent Deformation in 2195 Al-Li Alloy, *Mater. Charact.*, 2021, **182**, p 1–17. (**in English**)
40. Y. Deng, Z.M. Yin, and F.G. Cong, Intermetallic Phase Evolution of 7050 Aluminum Alloy during Homogenization, *Intermetallics*, 2012, **26**, p 114–121. (**in English**)
41. K.K. Ma, H.M. Wen, T. Hu, T.D. Topping, D. Isheim, D.N. Seidman, E.J. Lavernia, and J.M. Schoenung, Mechanical Behavior and Strengthening Mechanisms in Ultrafine Grain Precipitation-Strengthened Aluminum Alloy, *Acta Mater.*, 2014, **62**, p 141–155. (**in English**)